ACS NANO

www.acsnano.org

ARTICLE

Active Learning Framework for Expediting the Search of Thermodynamically Stable MXenes in the Extensive Chemical Space

Jaejung Park, Jongmok Lee, Jaejun Lee, Kyoungmin Min, Haesun Park,* and Seungchul Lee*

Cite This: https://doi.org/10.1021/acsnano.4c08621

Read Online

ACCESS | Metrics & More | Article Recommendations | Supporting Information

ABSTRACT: MXenes possess a wide range of materials properties owing to their compositional and stoichiometric diversities, facilitating their utilization in various technological applications such as electrodes, catalysts, and supercapacitors. To explore their applicability, identification of thermodynamically stable and synthesizable MXenes should precede. The energy above the convex hull (E^{hull}) calculated using the density functional theory (DFT) is a powerful scale to probe the thermodynamic stability. However, the high calculation cost of DFT limits the search space of unknown chemistry. To address this challenge, this study proposes an active learning (AL) framework consisting of a surrogate model and utility function for expeditious identification of thermodynamically stable MXenes in the extensive chemical space of 23,857 MXenes with compositional and stoichiometric diversity. Exploiting the fast inference speed and the capability of the AL framework to accurately identify stable MXenes, only 480 DFT calculations were required to identify 126 thermodynamically stable MXenes; among these, the stabilities of 89 MXenes have not been previously reported. In contrast, only two stable MXenes were identified among randomly selected 1693 MXenes, demonstrating the inefficiency of using only DFT calculations in exploring a large chemical space. The AL framework successfully minimized the number of DFT calculations while maximizing that of thermodynamically stable MXenes identified and can contribute to future studies in finding stable MXenes expeditiously.

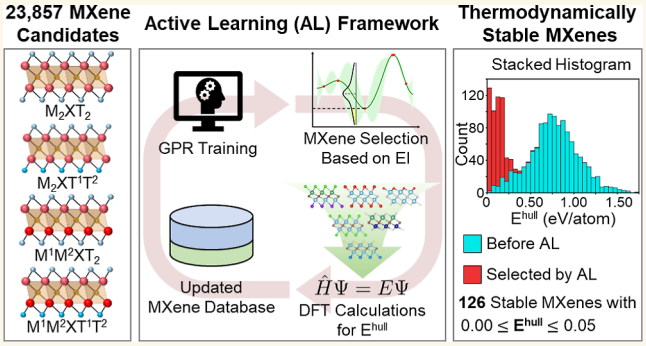

KEYWORDS: *MXene, thermodynamic stability, machine learning, active learning, density functional theory calculation*

MXenes[1] stand as a captivating domain in the field of two-dimensional (2D) materials, primarily owing to their compositional tunability. This feature has catalyzed their applications in energy storage,[2,3] electrocatalysis,[4,5] and water purification,[6−8] all of which are underpinned by their superior chemical, electronic, and adsorption properties. Comprising transition metal carbides, nitrides, and carbonitrides, MXenes are typically represented by the general formula $M_{n+1}X_nT_x$. Here, M, X, and T indicate transition metals, carbon and/or nitrogen, and surface terminations, respectively. Additionally, n denotes the number of carbon or nitrogen layers present in the MXene, and x represents the number of surface terminations attached to it. MXenes are distinct from conventional 2D materials in that they possess an extensive chemical space, which is attributed to their diverse combination of constituent elements (i.e., compositional tunability) and the presence of varied nonstoichiometric MXenes. Consequently, because of their compositional and stoichiometric flexibilities, MXenes are known to be the family of 2D materials with the largest chemical space.[9]

The large chemical space of MXenes, however, limits their comprehensive experimental exploration for various applications. To address this, high-throughput computational simulations that are represented by first-principles calculations like density functional theory (DFT) calculations, help guide experimental efforts by pinpointing optimal MXenes with targeted properties.[10−12] In line with this effort, numerous studies on MXenes have been conducted using DFT to predict

Received: June 27, 2024
Revised: September 23, 2024
Accepted: September 27, 2024

their electronic,[13] thermodynamic,[14] and mechanical properties.[15]

Among the various materials properties that can be explored through first-principles calculations, thermodynamic stability, particularly phase stability, quantified by the energy above the convex hull (E^{hull}), should be evaluated as a preliminary step to facilitate the further application of MXenes. E^{hull} is the energy difference between the formation energy of the unknown structure and the lowest formation energy configurations represented by the vertices of the convex hull in a phase diagram. When E^{hull} is zero, the compound is deemed stable against decomposition into competing phases. Positive E^{hull} values suggest potential metastable compounds, with smaller E^{hull} values often indicating the synthesizability of unknown structures. Therefore, in research focused on iodine-terminated MXenes with high synthesizability,[14] MXene semiconductors,[15] MXenes for energy storage materials,[16] and many others,[17−19] their stabilities were first assessed with DFT before proceeding to determine other relevant properties such as band gap and lithium storage capacities. Thus, E^{hull} is of paramount importance for MXene synthesis and applications.

Despite the tremendous utility of first-principles calculations, they remain limited when exploring the extensive chemical space of MXenes. This limitation stems from the fact that DFT calculations are computationally expensive and require large amounts of computational resources to thoroughly explore the chemical space of MXenes. Hence, previous studies examined only a limited portion of the extensive chemical space of MXenes in terms of both composition and stoichiometry, focusing only on MXenes with O surface termination,[5] Ti or V in M site,[20] and fixed chemical formula of $M'_2M''C_2T_2$.[21]

To overcome the massive computational demand of first-principles approaches, recent researches in fields of materials screening and cheminformatics have been actively applying artificial intelligence (AI), utilizing various approaches like machine learning (ML), artificial neural networks, and transformers in predicting materials properties that include thermodynamic, electric, and chemical properties.[22−28] Specifically, many studies have applied ML to assess the thermodynamic stability of MXenes, successfully identifying stable MXenes by predicting their thermodynamic properties. For instance, Park et al.[29] used ML regression and voting methods to analyze thermodynamic properties and identified 45 thermodynamically stable MXenes. Similarly, Vertina et al.[30] developed a regressor using an ML model to predict the thermodynamic properties of MXenes and He and Zhang[31] utilized a support vector machine (a type of ML) to classify the stability of MXenes.

Yet, these ML-based studies on the thermodynamic stability of MXenes face two challenges when exploring the large chemical space of MXenes.

(1) ML encounters difficulties with exploration due to its lack of consideration for uncertainty in predictions.

Since the ML model predicts thermodynamic properties (e.g., E^{hull}) based on those of the stable/unstable MXenes in the training data, the uncertainty for predictions of MXenes that have different compositions or stoichiometries compared to those in the training data would be very high. Due to this high uncertainty, these MXenes are worth investigating rather than relying solely on ML. However, if only ML is used, these MXenes might be discarded based on highly uncertain results. In other words, ML methods tend to find MXenes similar to the stable ones in the training data, potentially overlooking stable MXenes with compositions and stoichiometries that were not present in the training data. This issue can be especially problematic when the training database contains a very small number of MXenes, such as the 85 MXenes used in the previous study.[31]

(2) ML does not inherently operate iteratively; it is a one-time process.

In studies utilizing ML, additional data is inevitably generated as the properties of materials selected by ML are verified using computational methods. By retraining ML models with this data and subsequently making predictions on the remaining materials, there is potential to discover additional materials with desired properties. Also, iteratively performing computations and retraining can further enhance the discovery. However, many ML-based studies do not employ this iterative retraining approach and in particular, in the previous work,[29] even though the E^{hull} values of 45 MXenes were additionally obtained through DFT calculations, they were not used to retrain ML.

To utilize uncertainties in ML predictions and to fully exploit additionally obtained data for a more thorough exploration of extensive chemical space, active learning (AL) has recently been employed in various studies. AL consists of two essential components: a surrogate model and utility function. The surrogate model serves as a substitute for experiments or first-principles calculations, enabling rapid prediction of material properties and, importantly, quantifying the uncertainty of each prediction. Next, the utility function accurately selects materials with a high probability of possessing desired properties based on predictions of the surrogate model and uncertainties of such predictions, making possible to investigate materials with feature values different from the training data. The actual material properties of the selected materials are then obtained through experiments or first-principles calculations. This data is further utilized to retrain the surrogate model, iteratively repeating the process of prediction−material selection−verification. Leveraging these features, AL has been applied to explore chemical spaces of ferroelectric perovskites,[32] thermoelectric materials,[33] solid-state electrolytes,[34] and iridium oxide polymorphs[35] and successfully identified desirable materials with comparably lower computational costs or less number of experiments.

Encouraged by the recent advances of AL in materials science, this study proposes an AL framework that consists of an ML surrogate model, a utility function, and DFT calculations to expedite the identification of thermodynamically stable MXenes with 0.00 eV/atom $\leq E^{hull} \leq$ 0.05 eV/atom in the extensive chemical space. With the fast inference speed of the surrogate model and the judicious MXene selection by the utility function, compositionally and stoichiometrically diverse 23,857 MXenes were studied as the targeted chemical space to explore. Compositionally, 11 transition metals and 14 types of surface terminations were considered. Stoichiometrically, not only iso-stoichiometric but also varied nonstoichiometric MXenes were included. Thus, this study leveraged the advantages of AL to consider a more diverse and numerically larger set of MXenes compared with those reported in previous studies, minimizing the number of DFT calculations and maximizing the number of stable MXenes identified. The demonstrated utility and efficiency of the AL framework are expected to assist subsequent research in

https://doi.org/10.1021/acsnano.4c08621
ACS Nano XXXX, XXX, XXX−XXX

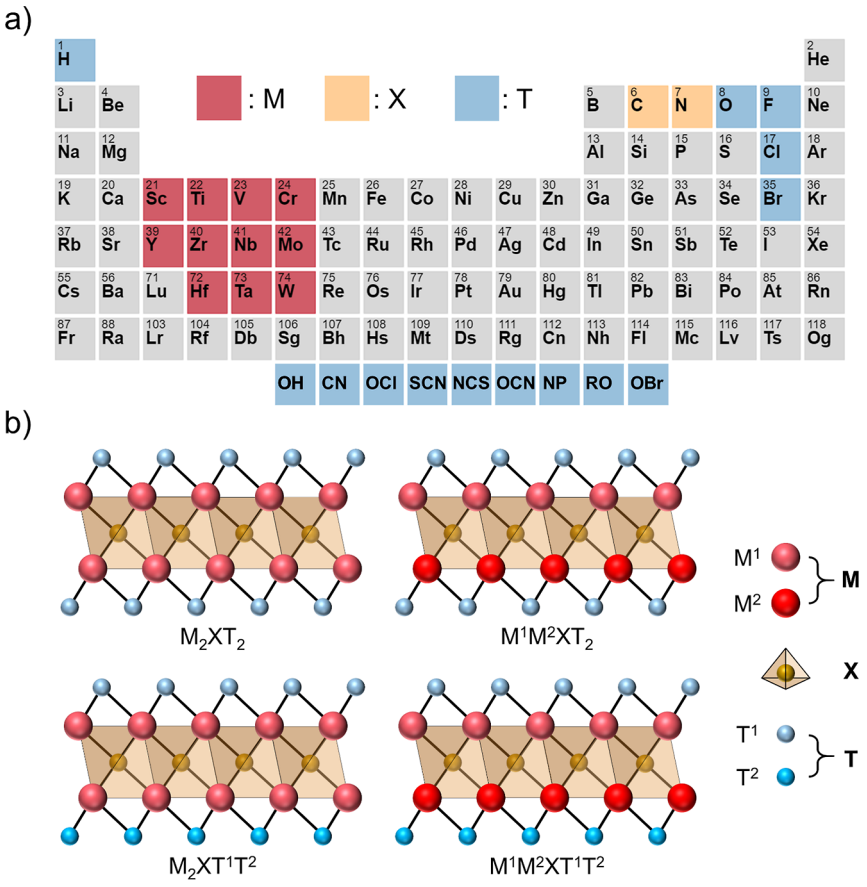

Figure 1. (a) Constituents of 23,857 MXenes represented on the periodic table (b) four different stoichiometries composing 23,857 MXenes.

identifying thermodynamically stable MXenes through ML and first-principles calculations.

RESULTS AND DISCUSSION

MXenes Structures and Chemical Space. In order to demonstrate the ability of the proposed AL framework to effectively and efficiently identify thermodynamically stable MXenes within an extensive chemical space, the MXene database provided by the aNANt group[36] was used as the target data set (i.e., target chemical space). The aNANt MXene database contains a compositionally and stoichiometrically diverse set of 23,857 MXenes. Compositionally, 11 different transition metals as well as 14 types of surface terminations were considered as the constituents of MXenes (Figure 1a). Stoichiometrically, not only iso-stoichiometric MXenes (M_2XT_2) but also three nonstoichiometric MXenes, namely, MXenes with two different transition metals ($M^1M^2XT_2$), two types of surface terminations ($M_2XT^1T^2$), and distinct transition metals and surface terminations ($M^1M^2XT^1T^2$) were included (Figure 1b). Importantly, the thermodynamic properties (i.e., E^{hull}) of the 23,857 MXenes provided by the aNANt group remain unexplored. Therefore, the aNANt MXene database was used as the target data set since it offers a comprehensive representation of the extensive chemical space of MXene.

Featurization. For the featurization of MXenes in the aNANt database, the chemical formulas of 23,857 MXenes were first extracted. Each MXene was then represented with 149 features, which were derived from its chemical formula using the matminer software.[37] These features represent varied characteristics from the chemical compositions of MXenes, including the ionic character between two constituent elements, average atomic radius of the constituent elements, and total number of valence electrons. The specifics of the 149 features utilized in this study can be found in the Supporting Information (SI.1).

Two additional preprocessing steps were performed after the featurization: (i) dimensionality reduction using principal component analysis (PCA) and (ii) one-hot encoding for the constituents of MXenes. Through PCA, the feature dimensions were reduced from 149 to 15. Subsequently, one-hot encoding was applied to represent 11 transition metals, 14 surface terminations, and two X site atoms, adding 27 dimensions to the previously reduced 15 dimensions by assigning the value of "1" to the features corresponding to the constituents (i.e., transition metals, surface terminations, and X site atoms) present in a MXene and a "0" to those that are absent. After completing the featurization process, each MXene was characterized by 42 features. Detailed explanations of PCA, one-hot encoding, and the rationale behind these preprocessing steps are provided in the Supporting Information (SI.2) and the implementation methods of matminer for featurization and two additional preprocessing steps are detailed in the Methods section.

Initial Database. To train the surrogate model included in the AL framework on the relationship between the 42 features and E^{hull} values, the initial database generation was performed. Thus, among the 23,857 MXenes, approximately 5% (1213 MXenes) had been chosen at random to determine their E^{hull} values using DFT calculations, the details of which are

https://doi.org/10.1021/acsnano.4c08621
ACS Nano XXXX, XXX, XXX−XXX

presented in the Methods section. The distribution of the DFT-calculated E^{hull} values for 1213 randomly selected MXenes that comprise the initial database is shown in Figure 2. Here, E^{hull} = 0 eV/atom indicates that the MXene is

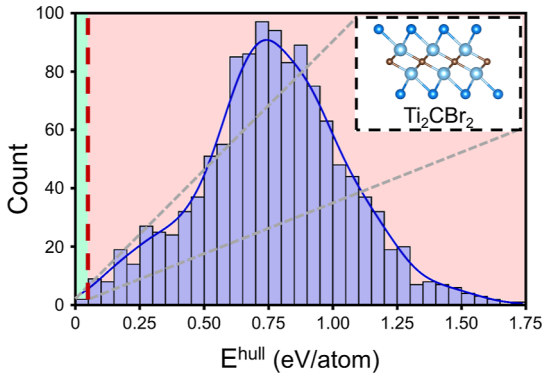

Figure 2. Distribution of energy above the convex hull (E^{hull}) values of 1213 MXenes comprising the initial database; the green zone represents the range of E^{hull} values that satisfy the thermodynamic stability criterion, while the red zone indicates the range that does not meet the criterion, representing the thermodynamically unstable region. The horizontal axis represents the values of E^{hull}, and each interval of the histogram corresponds to a range of 0.05 eV/atom of E^{hull}; the vertical axis represents the number of MXenes within each range of E^{hull} values. Among 1213 MXenes, only one MXene, Ti_2CBr_2, satisfied the thermodynamic stability criterion; its structure is presented in the upper right corner.

thermodynamically stable, implying that it will not decompose to other competing stable phases. 0 eV/atom < E^{hull} ≤ 0.05 eV/atom indicates that the MXene is in a metastable state, whereas E^{hull} > 0.05 eV/atom implies that the MXene is unstable. Out of the 1213 MXenes examined, only one MXene, Ti_2CBr_2, was stable with E^{hull} = 0 eV/atom, and none was metastable. The E^{hull} values of the remaining 1212 MXenes ranged up to 1.73 eV/atom, and the average E^{hull} of all the 1213 MXenes was high at 0.77 eV/atom. The workflow of both featurization and initial database generation is presented in the Supporting Information (SI.3).

AL Framework. The AL framework presented in this study proceeds through the following steps and an overview of the framework is shown in Figure 3:

1. Gaussian process regression (GPR), serving as the surrogate model within the AL framework, learns the relationship between the 42 features and E^{hull} values using the training database.
2. With the trained GPR, predictions are made for MXenes whose E^{hull} values have not yet been calculated using DFT, providing both the predicted E^{hull} values and uncertainties of such predictions.
3. By utilizing these values in the expected improvement (EI) utility function, 40 MXenes with highest EI values (i.e., predicted to exhibit lower E^{hull} values to a significant extent) are chosen from the unlabeled pool.
4. DFT calculations are conducted on these 40 MXenes to determine their precise E^{hull} values.
5. The training database is then updated by adding these 40 MXenes for a subsequent iteration.
6. Steps 1 to 5 are repeated until no more than two thermodynamically stable MXenes are found during each of the three consecutive iterations.

The AL framework was initiated by training the GPR surrogate model using the initially calculated 1213 MXenes. To evaluate the performance of the AL framework, additional 40 MXenes were randomly selected in Step 3. For these 40 MXenes, the E^{hull} values were also obtained through DFT calculations, and the results were compared with the E^{hull} values of the 40 MXenes selected by the AL framework in each iteration. Specifically, 40 MXenes selected using two different methods (i.e., random and AL framework) were compared in terms of their average E^{hull} values and the number of thermodynamically stable MXenes with 0.00 eV/atom ≤ E^{hull} ≤ 0.05 among them. However, randomly selected MXenes were used solely for comparative purposes and were not added to the training database.

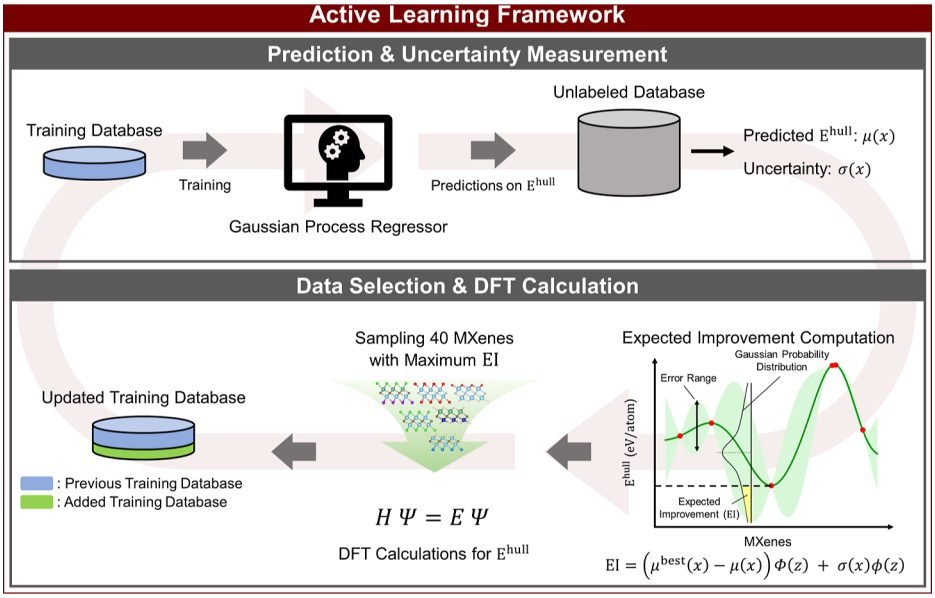

Figure 3. Workflow of the AL framework proposed in this study.

https://doi.org/10.1021/acsnano.4c08621
ACS Nano XXXX, XXX, XXX−XXX

As shown in the steps of the AL framework, the key components are the surrogate model and the utility function, with GPR and EI employed as the respective components. First, GPR is a nonparametric, Bayesian regression method, that uses a set of prior probability distributions to predict an output for a given input, leveraging kernel functions, whose details are given in Table 1, to determine relationship between data points. The reasons for adopting GPR as the surrogate model include: (1) for the utility function to be effective, predictions and their associated uncertainties are required. GPR is among the few ML algorithms capable of providing both of them; (2) due to its kernel-based approach, GPR can adeptly learn the nonlinear relationships between the 42 features and E^{hull}, as confirmed in performance comparison tests with other ML models; the method and results of the performance comparison test are detailed in the Supporting Information (SI.4).

Table 1. Details About Hyperparameters of Gaussian Process Regressor, Kernel Function, and EI Equation[a]

Gaussian process regressor
kernel = kernel, $n\_restarts\_optimizer$ = 40, normalize_y = false, random_state = 10
kernel
kernel = ConstantKernel (1.0, $(10^{-3},10^{3})$) × Matern ([1.0] × 42, $[[10^{-3},10^{3}]]$ × 42, 1.5) + WhiteKernel (1.0, $(10^{-3},10^{3})$)
expected improvement
$EI = (\mu^{best}(x) - \mu(x))\Phi(z) + \sigma(x)\phi(z)$ where $z = \frac{(\mu^{best}(x) - \mu(x))}{\sigma(x)}$

[a] $\mu^{best}(x)$: smallest target value in training database, $\mu(x)$: mean of predicted values, $\sigma(x)$: standard deviation of predicted values, ϕ: standard Gaussian distribution function, Φ: standard cumulative distribution function.

Second, EI, whose specific equation is given in Table 1, balances the use of "exploration" and "exploitation" strategies to determine which MXene is promising for conducting DFT calculations. To explain in more detail through the EI equation, the first term is related to exploitation. The exploitation strategy focuses on targeting MXenes predicted to have low E^{hull} values, and the $(\mu^{best}(x) - \mu(x))$ part of the first term helps facilitate this. $(\mu^{best}(x) - \mu(x))$ indicates how much lower the predicted E^{hull} value $(\mu(x))$ of an MXene is compared to that of the MXene with the smallest E^{hull} value within the training database $(\mu^{best}(x))$. The smaller the predicted E^{hull} value compared to $\mu^{best}(x)$, the larger the size of the first term, resulting in a higher EI value. When $\mu(x)$ is greater than $\mu^{best}(x)$, it acts as a sort of penalty term, allowing the EI values of MXenes where $\mu(x)$ is close to $\mu^{best}(x)$ to be larger. By multiplying $(\mu^{best}(x) - \mu(x))$ and standard cumulative distribution function (CDF) value of "z", which is the standardized value of $\mu^{best}(x)$ based on the $\mu(x)$ and the prediction uncertainty, the first term performs the role of exploitation. The visual illustration of the first term can be found in the Supporting Information (SI.5), which also describes the meaning of the standard CDF. Next, the second term of the EI equation is related to exploration. The exploration strategy focuses on targeting MXenes with high uncertainty in predictions, based on the idea that many stable MXenes might exist in unexplored chemical spaces, and to

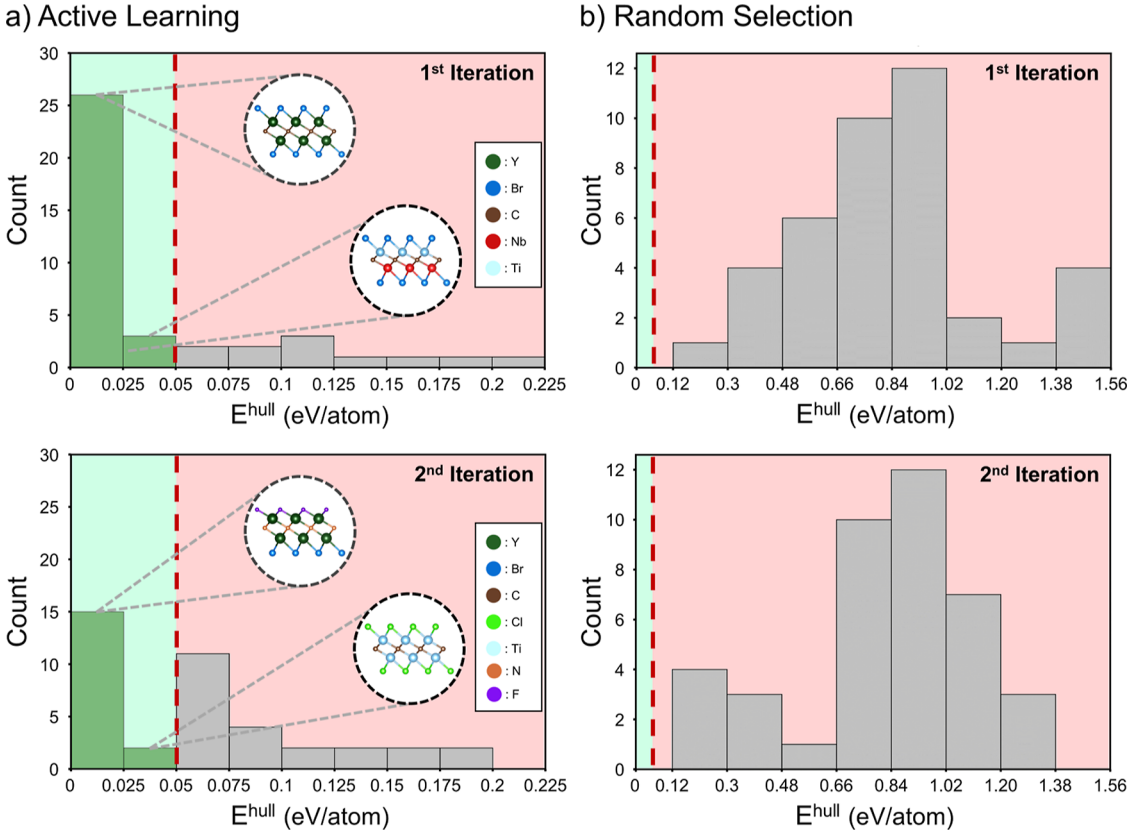

Figure 4. Distributions of energy above the convex hull values of (a) AL queried and (b) randomly selected MXenes compared for the first two AL iterations. The green zone represents thermodynamic stability or metastability, while the red zone indicates instability.

https://doi.org/10.1021/acsnano.4c08621
ACS Nano XXXX, XXX, XXX−XXX

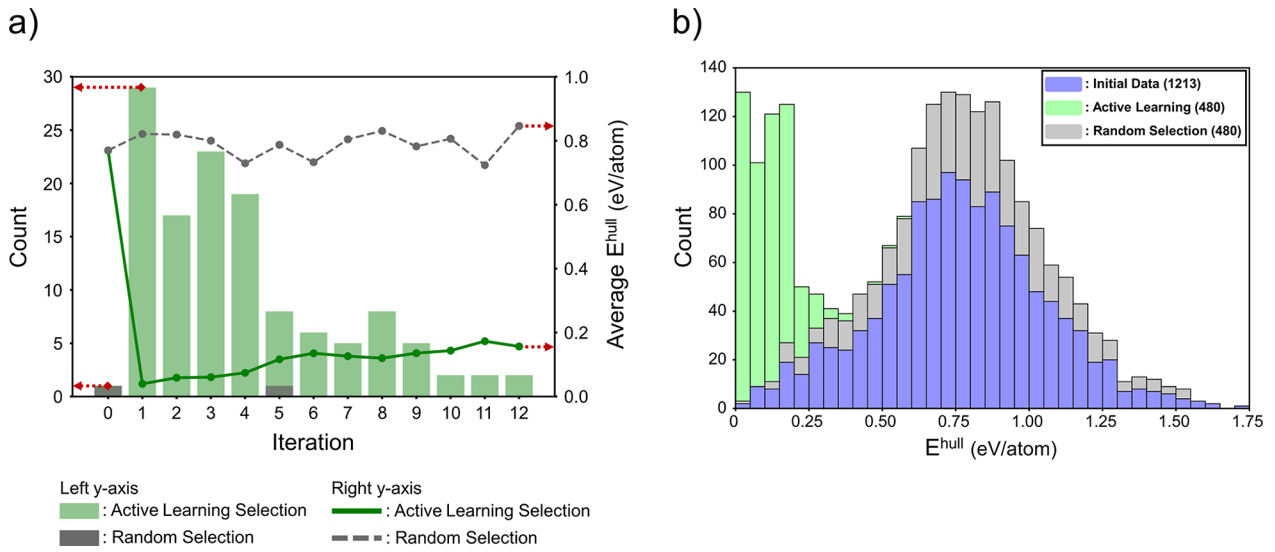

Figure 5. (a) Average energy above the convex hull values of 40 MXenes selected by the AL framework and the number of MXenes that satisfy the thermodynamic stability criteria recorded for all 12 iterations and the same values computed from 40 randomly selected MXenes (b) stacked histogram of energy above the convex hull values of 2173 MXenes comprising 1213 MXenes from the initial database, 480 MXenes selected by AL framework, and 480 randomly selected MXenes; the blue histogram corresponding to the 1213 MXenes from the initial database was first plotted, with the gray histogram corresponding to the 480 randomly selected MXenes stacked on top of it, and the green histogram corresponding to the 480 MXenes selected by the AL framework stacked on top of the blue and gray histograms.

learn more about the unknown relationship between the 42 features of MXenes and E^{hull}. $\sigma(x)$ represents the prediction uncertainty for the E^{hull} value of an MXene. A large $\sigma(x)$ implies that the input feature exhibits different characteristics compared to the data used in training, indicating that it is worth investigating further. Consequently, the larger $\sigma(x)$, the greater the second term becomes, resulting in a higher EI value. By multiplying $\sigma(x)$ with the standard Gaussian distribution function value of z, it fulfills the role of exploration. The visual illustration of the second term can also be found in the Supporting Information (SI.5), where the meaning of the standard Gaussian distribution function is described. By summing the terms responsible for exploitation and exploration, the EI value is obtained, allowing a balanced consideration of both exploitation and exploration strategies. A high EI value signifies not only a high probability that the MXene has a low E^{hull} value but also that it could be a MXene, possessing different characteristics from those in the training database, making it useful for finding stable MXenes that have different compositions or stoichiometries compared to those in the training data in unexplored chemical space where the majority are unstable. The implementation methods for both GPR surrogate model and EI utility function are described in detail in the Methods section.

First Two Iterations of AL. The distributions of the E^{hull} values of the MXenes selected by the AL framework and those chosen randomly for the first two AL iterations are presented in Figure 4. In the first iteration (Figure 4a), of the 40 MXenes selected by the AL framework, 29 (73%) met the thermodynamic stability criteria (i.e., 0.00 eV/atom $\leq E^{hull} \leq$ 0.05 eV/atom), of which 17 were stable with E^{hull} = 0 eV/atom and the remaining 12 were metastable. Furthermore, the average E^{hull} value for the 40 MXenes was low, at 0.04 eV/atom. In contrast, none of the 40 MXenes selected at random satisfied the stability condition, with an average E^{hull} value of 0.82 eV/atom. In essence, while only one stable MXene was found after conducting DFT calculations of the E^{hull} values for 1213 MXenes, and none was identified after randomly selecting an additional 40, a single AL iteration enabled the discovery of 29 stable MXenes with only 40 DFT calculations. Subsequently, after adding the E^{hull} values of the 40 MXenes calculated in the first iteration to the training database, the second iteration (Figure 4b) was conducted, identifying 17 thermodynamically stable MXenes. Eleven MXenes were stable with E^{hull} = 0 eV/atom; the remaining six MXenes were metastable. Moreover, the average E^{hull} value for the 40 MXenes was low, at 0.06 eV/atom. However, that of 40 randomly selected MXenes was high at 0.82 eV/atom, and not even one MXene met the thermodynamic stability criterion, demonstrating the efficacy of the AL framework.

Overall Iterations of AL. The AL iterations were terminated at the 12th iteration because the number of thermodynamically stable MXenes found in three consecutive iterations, including the 12th iteration, was two or fewer, respectively, indicating that the thermodynamically stable MXenes were likely depleted in the chemical space. Figure 5a depicts the average E^{hull} value and number of MXenes satisfying the thermodynamic stability criterion for the 40 MXenes selected by the AL framework in each of the 12 iterations. For comparison, the figure also presents the same quantities for 40 MXenes randomly selected at each iteration. The average E^{hull} values for the 40 MXenes selected by the AL framework ranged low from 0.04 to 0.17 eV/atom during 12 iterations, whereas those randomly selected exhibited much larger values ranging from 0.72 to 0.85 eV/atom. Additionally, using only 480 DFT calculations, the AL framework identified 126 thermodynamically stable MXenes, whereas the random selection method found only one with the same computational cost. Particularly, the thermodynamically stable MXene discovered in the fifth iteration through the random selection method, V_2CCl_2 with an E^{hull} value of 0.007 eV/atom, was also identified by the AL framework in the 12th iteration and was included among the 126 thermodynamically stable MXenes, demonstrating the AL framework's precision in finding stable

https://doi.org/10.1021/acsnano.4c08621
ACS Nano XXXX, XXX, XXX−XXX

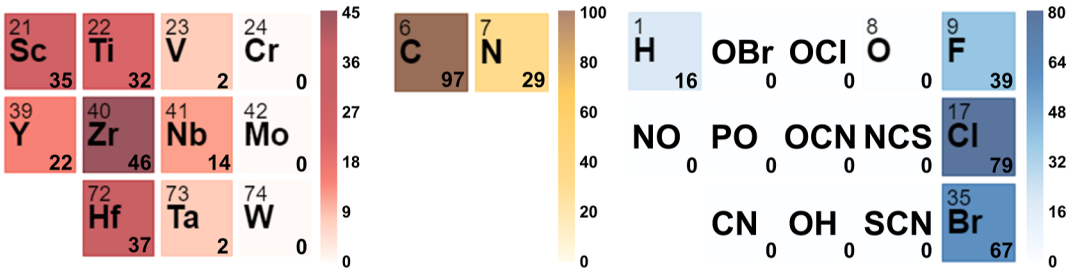

Figure 6. Constituents of the thermodynamically stable 126 MXenes; the red, yellow, and blue colorbars next to the transition metals, X site atoms, and surface terminations indicate the number of MXenes among the 126 that contain each constituent. Darker colors signify a higher number of MXenes containing that constituent, and the numbers displayed bottom right corner of each constituent represent the count of MXenes with that constituent. If MXenes have two different transition metals or two different surface terminations, the count is incremented by one for each constituent.

MXenes across an extensive chemical space. Of these 126 MXenes, 89 MXenes had not been evaluated for their stability in previous studies, indicating the efficacy of the AL framework in finding stable MXenes; the access method for the E^{hull} values of the 126 MXenes is summarized in the Supporting Information (SI.6). Furthermore, Figure 5b represents the stacked histogram of the E^{hull} values of 2173 MXenes, obtained after 12 AL iterations. It is confirmed once again that a significant number of the 480 MXenes randomly selected during the 12 AL iterations and the 1213 MXenes from the initial database have high E^{hull} values, forming a nearly normal distribution with respect to their average value (0.77 eV/atom). In contrast, the E^{hull} values of the 480 MXenes selected by the AL framework are all clustered at lower values, indicating the usefulness of the AL framework in identifying stable MXenes. The access method for the E^{hull} values of the 2173 MXenes is described in the Supporting Information (SI.7).

Composition-Wise and Stoichiometric-Wise Analysis. The frequency of the constituents of the 126 MXenes is summarized in Figure 6. First, 94% of the 126 MXenes had Group-3 and/or Group-4 transition metals, while 77% of them were carbides having C in the X site. These results are consistent with those reported previously. For example, Li et al.[38] listed successfully synthesized MXenes, noting a high prevalence of Group-3 and Group-4 transition metal-based MXenes at 57%. Furthermore, approximately 84% of them were carbides. This confirms that the 126 MXenes exhibit a chemical composition trend similar to that of the MXenes successfully synthesized in previous studies. Next, as for the surface terminations of the 126 MXenes, elements from Group-17 (i.e., halogen atoms) were predominantly observed. This can be understood in terms of the relative electronegativity of the transition metals with the surface terminations. The interaction between the transition metal of MXene and the surface termination plays a crucial role in stability, depending on the electronegativity difference between them.[39] A large electronegativity difference enables a strong interaction, and the bond between the halogen surface termination and Group-3 or Group-4 transition metals (i.e., early transition metals) maximizes this difference. Moreover, Wyatt et al.[40] obtained the bond energies of various transition metals and surface terminations of MXenes, and they identified that the bond energies of early transition metals and surface terminations with halogen elements, particularly F and Cl, were higher than those of other bonds. This implies that the interaction between them is strong and requires a significant amount of energy for decomposition, indicating high stability. In summary, the 126 MXenes identified through the AL framework exhibited a chemical composition trend similar to that of the successfully synthesized MXenes, particularly in the presence of Group-3 and Group-4 transition metals and C at the X site. Additionally, their stability could be theoretically explained by the large electronegativity difference and strong bond energy between the halogen surface terminations and Group-3 and Group-4 transition metals.

Across the four different stoichiometries considered in this study, 126 MXenes exhibited a nearly even distribution; the frequencies of the stoichiometries are listed in Table 2. First,

Table 2. Number of MXenes for Each of Four Different Stoichiometries

total thermodynamically stable MXenes			
126			
iso-stoichiometric MXenes	nonstoichiometric MXenes		
M_2XT_2	$M^1M^2XT_2$	$M_2XT^1T^2$	$M^1M^2XT^1T^2$
25	26	37	38

there were 25 iso-stoichiometric MXenes, all of which have been previously reported to be thermodynamically stable by first-principles calculations.[29,41−43] Also, iso-stoichiometric MXenes having surface terminations with halogen elements have been successfully synthesized,[44−46] suggesting the higher probability of their synthesis in future studies than that of other stoichiometries. Second, there were 26 MXenes with two different transition metals ($M^1M^2XT_2$), and only one of them, $ScYCF_2$, was previously known for its stability.[47] Because MXenes with two different transition metals have been successfully synthesized (although they did not have halogen surface termination)[48−50] and because the methods for terminating MXenes with halogen atoms have been clarified in previous studies, the 26 MXenes with two different transition metals can also be considered to have high synthesizability. Finally, 75 MXenes with two different surface terminations ($M_2XT^1T^2$) and distinct transition metals and surface terminations ($M^1M^2XT^1T^2$) were identified, among which the thermodynamic stabilities of only 11 MXenes have been previously confirmed through first-principles calculations.[51,52] While extensively studied through various computational methods,[53−55] these MXenes have not yet been successfully synthesized, due to the complexities involved in obtaining different surface terminations on their top and bottom surfaces. However, syntheses of other 2D materials,

https://doi.org/10.1021/acsnano.4c08621
ACS Nano XXXX, XXX, XXX−XXX

such as MoSSe,[56] WSSe,[57] Janus graphene with halogen surface termination on the top and oxygen-functional groups at the bottom,[58] and Janus graphene oxide with Pt on one surface and TiO_2 on the other,[59] have been reported to be successful, despite the asymmetry of the top and bottom surfaces. Hence, additional studies are required to utilize these synthesis methods for MXenes with stoichiometries of $M_2XT^1T^2$ and $M^1M^2XT^1T^2$. In conclusion, while previous computational studies have often focused on MXenes with a single stoichiometry, primarily iso-stoichiometric MXenes, this study used the AL framework to consider various stoichiometries at the same time. This demonstrates the ability of the AL framework to account for not only the compositional but also the stoichiometric diversity of MXenes, a capability that can facilitate the discovery of stable MXenes with asymmetric structures.

The great quantity and diversity of thermodynamically stable MXenes identified in this study can be attributed to the advantages of AL; its ability to consider the uncertainty of predictions and to operate iteratively. The contributions of each advantage of AL can be summarized in two key points, and the superiority of the AL method can also be demonstrated through a comparison with the previous ML study. First, the ability to account for uncertainty enabled the identification of 126 thermodynamically stable MXenes, even though there was only one stable MXene in the initial database. EI, the utility function used in this study, considers not only the MXenes predicted to have low E^{hull} values but also those with high uncertainty in their predictions as worth investigating. Thus, EI could select stable MXenes with various compositions and stoichiometries that showed different characteristics from MXenes used in the training. This enabled the discovery of stable MXenes that were stoichiometrically and compositionally different from the Ti_2CBr_2, the only stable MXene in the initial training database. For comparison, the previous ML study[29] that screened same MXene candidates regarding thermodynamic stability did not consider uncertainties of predictions and, therefore, could only identify MXenes with characteristics similar to stable 2D materials in the training database. In particular, in the case of nonstoichiometric MXenes, only 6 were discovered; while this study was able to find 101 nonstoichiometric MXenes, including those 6. Moreover, the iterative nature of AL enabled the training database to be continuously updated with additionally calculated MXenes, leading to the discovery of more than 10 stable MXenes in second, third, and fourth iterations. In contrast, the previous work[29] employed ML to perform only a single screening, identifying 45 stable MXenes, with an E^{hull} value threshold of 0.1 eV/atom. Among them, MXenes with E^{hull} values below 0.05 eV/atom were all identified in this study as well. Overall, the use of AL enabled a practical exploration on the extensive chemical space of MXenes by accounting for prediction uncertainty and allowed for a more thorough investigation through iterative updates to the training data.

CONCLUSIONS

The AL framework presented in this study was composed of a GPR surrogate model and an EI utility function. The fast learning and prediction capabilities of GPR combined with the discerning power of the EI utility function enabled the consideration of a wide range of stoichiometrically and compositionally diverse MXenes, thus leading to the accurate and expeditious identification of thermodynamically stable MXenes. A total of 126 thermodynamically stable MXenes were discovered through 12 AL iterations, which involved 480 DFT calculations. Furthermore, the average E^{hull} values of the 40 MXenes selected by the AL framework in each iteration were low, ranging from 0.04 to 0.17 eV/atom. In contrast, out of the 480 MXenes randomly selected during the 12 AL iterations and 1213 MXenes randomly chosen for the initial database, only two MXenes were found to be thermodynamically stable. Particularly, the average E^{hull} values of the 40 randomly selected MXenes in each iteration were high, ranging from 0.72 to 0.85 eV/atom. This demonstrates that thermodynamically stable MXenes are extremely scarce within the explored chemical space of this study, and attempting to explore this extensive chemical space solely through DFT calculations would be highly inefficient. However, the AL framework effectively minimizes the number of DFT calculations while maximizing the discovery of thermodynamically stable MXenes. In conclusion, the present study demonstrated the utility of employing an AL framework to search for materials with targeted properties within an extensive chemical space by focusing the effort on candidates with higher priority. This approach extends beyond screening MXenes based on thermodynamic properties, encompassing screening for various kinetic properties, such as ionic or thermal conductivity. Moreover, it can be applied to more diverse types of MXenes, including those with different atomic stackings, e.g., ABA stacking, and high entropy MXenes with extensive chemical variability. Regarding further future research directions, there are two main areas for improvement in the AL framework proposed in this study. First, the surrogate model lacks explainability regarding which features it primarily leverages to predict the E^{hull} values of MXene. Ensuring the explainability of predictions would provide valuable insights into the relationship between input features and E^{hull}. Therefore, it may be beneficial to consider using explainable AI techniques, including Shapley Additive Explanations and attention weight visualization of transformer models, as demonstrated in previous studies.[27,60,61] Second, additional screening methods will be necessary depending on the applications of the stable MXenes. For example, if the goal is to identify MXene catalyst candidates, the proposed framework can be initially used to quickly find stable MXenes, after which DFT calculations should be employed to verify catalyst properties. However, DFT calculations have limitations in observing the spatiotemporal evolution of active sites in catalyst. Therefore, kinetic analysis using kinetic Monte Carlo simulations, as done in previous computational studies,[62−64] will be necessary. These additional screening steps would enable the proposal of MXene catalysts that are both stable and highly effective.

METHODS

Data Processing and AL. The featurization of MXene was conducted using five featurizers from matminer: ElementProperty, ValenceOrbital, Stoichiometry, IonProperty, and TMetalFraction, resulting in a total of 149 features. To reduce the dimensionality of these 149 features to 15, PCA was applied using the PCA function from the "decomposition" module in Scikit-Learn package. The final 42 features were formed by concatenating 27 features created through one-hot encoding, which was implemented using a custom automated code written in Python. The GPR surrogate model that constitutes the AL framework was developed using the GaussianProcessRegressor function from the "gaussian_process" module in Scikit-Learn, with a kernel combining RBF, ConstantKernel, and WhiteKernel from the

https://doi.org/10.1021/acsnano.4c08621
ACS Nano XXXX, XXX, XXX−XXX

same module. The EI utility function was implemented in Python by directly expressing the mathematical formula using NumPy and SciPy packages.

DFT Calculations. The E^{hull} values of MXenes that comprise the initial database and are chosen by the AL framework were generated via DFT calculations in conjunction with the Materials Project (MP) database[65] interfaced with the Python Materials Genomics (pymatgen) code.[66] DFT calculations[67] were performed as implemented in Vienna Ab initio Simulation Package.[68] The core−valence electron interaction was treated by the projector-augmented wave potential,[69,70] and the plane-wave basis set with a cutoff energy of 520 eV was used. The electron exchange−correlation functional of the generalized gradient approximation formulated by Perdew−Burke−Ernzerhof was adopted.[71] The Hubbard U correction was employed for the compounds containing transition metals with delocalized d-orbital electrons, and the U values were chosen to closely match the experimental formation energy. The U values were taken from the literature.[72] The k-points mesh was constructed with the pymatgen code[66] with a density of 1500/reciprocal atom. The phase diagram was calculated using the DFT-calculated energies of the relevant compounds obtained from the MP database.[65]

ASSOCIATED CONTENT

Data Availability Statement

The access method for the energy above the convex hull values of 2173 MXenes explored in this study is described in the Supporting Information.

Supporting Information

The Supporting Information is available free of charge at https://pubs.acs.org/doi/10.1021/acsnano.4c08621.

> Supporting Information regarding features, details of dimensionality reduction and one-hot encoding, workflow of preprocessing, performance validation of GPR, visual representation of EI utility function, and access methods for energy above convex hull values of 126 thermodynamically stable MXenes and 2173 MXenes (PDF)

AUTHOR INFORMATION

Corresponding Authors

Haesun Park − *School of Integrative Engineering, Chung-Ang University, Seoul 06974, Republic of Korea;* orcid.org/0000-0001-6266-8151; Email: parkh@cau.ac.kr

Seungchul Lee − *Department of Mechanical Engineering, Korea Advanced Institute of Science and Technology (KAIST), Daejeon 34141, Republic of Korea;* orcid.org/0000-0002-1034-1410; Email: seunglee@kaist.ac.kr

Authors

Jaejung Park − *Department of Mechanical Engineering, Korea Advanced Institute of Science and Technology (KAIST), Daejeon 34141, Republic of Korea;* orcid.org/0009-0006-7962-3105

Jongmok Lee − *Department of Mechanical Engineering, Pohang University of Science and Technology (POSTECH), Pohang 37673, Republic of Korea*

Jaejun Lee − *Department of Mechanical Engineering, Pohang University of Science and Technology (POSTECH), Pohang 37673, Republic of Korea;* orcid.org/0009-0003-8878-1752

Kyoungmin Min − *School of Mechanical Engineering, Soongsil University, Seoul 06978, Republic of Korea;* orcid.org/0000-0002-1041-6005

Complete contact information is available at: https://pubs.acs.org/10.1021/acsnano.4c08621

Notes

The authors declare no competing financial interest.

ACKNOWLEDGMENTS

This research was supported in part by the Nano & Material Technology Development Program through the National Research Foundation of Korea (NRF) funded by Ministry of Science and ICT (RS-2024-00451579) and by the National Research Foundation of Korea (NRF) grant funded by the Korea government (MSIT) (no. 2022R1C1C1011660).

REFERENCES

(1) Naguib, M.; Kurtoglu, M.; Presser, V.; Lu, J.; Niu, J.; Heon, M.; Hultman, L.; Gogotsi, Y.; Barsoum, M. W. Two-Dimensional Nanocrystals Produced by Exfoliation of Ti3AlC2. In *MXenes*; Jenny Stanford Publishing, 2011; pp 15−29.

(2) Anasori, B.; Lukatskaya, M. R.; Gogotsi, Y. 2D Metal Carbides and Nitrides (MXenes) for Energy Storage. *Nat. Rev. Mater.* **2017**, *2*, 16098.

(3) Zhou, M.; Shen, Y.; Liu, J.; Lv, L.; Gao, X.; Zhang, Y.; Meng, X.; Yang, X.; Zheng, Y.; Zhou, Z. Superionic Conductivity and Large Capacitance Behaviors of Two-Metal MXenes WCrC in Sodium Ion Battery. *Vacuum* **2022**, *200*, 111054.

(4) Seh, Z. W.; Fredrickson, K. D.; Anasori, B.; Kibsgaard, J.; Strickler, A. L.; Lukatskaya, M. R.; Gogotsi, Y.; Jaramillo, T. F.; Vojvodic, A. Two-Dimensional Molybdenum Carbide (MXene) As an Efficient Electrocatalyst for Hydrogen Evolution. *ACS Energy Lett.* **2016**, *1*, 589−594.

(5) Kan, D.; Wang, D.; Cheng, Y.; Lian, R.; Sun, B.; Chen, K.; Huo, W.; Wang, Y.; Chen, G.; Wei, Y. Designing of Efficient Bifunctional ORR/OER Pt Single-Atom Catalysts Based on O-Terminated MXenes by First-Principles Calculations. *ACS Appl. Mater. Interfaces* **2021**, *13*, 52508−52518.

(6) Meidani, K.; Cao, Z.; Barati Farimani, A. Titanium Carbide MXene for Water Desalination: A Molecular Dynamics study. *ACS Appl. Nano Mater.* **2021**, *4*, 6145−6151.

(7) Zhang, B.; Wong, P. W.; An, A. K. Photothermally Enabled MXene Hydrogel Membrane with Integrated Solar-Driven Evaporation and Photodegradation for Efficient Water Purification. *Chem. Eng. J.* **2022**, *430*, 133054.

(8) Zhang, Y.; Chen, X.; Luo, C.; Gu, J.; Li, M.; Chao, M.; Chen, X.; Chen, T.; Yan, L.; Wang, X. Column-to-Beam Structure House Inspired MXene-Based Integrated Membrane with Stable Interlayer Spacing for Water Purification. *Adv. Funct. Mater.* **2022**, *32*, 2111660.

(9) Zhan, C.; Sun, W.; Xie, Y.; Jiang, D.-e.; Kent, P. R. Computational Discovery and Design of MXenes for Energy Applications: Status, Successes, and Opportunities. *ACS Appl. Mater. Interfaces* **2019**, *11*, 24885−24905.

(10) Guo, Z.; Zhou, J.; Si, C.; Sun, Z. Flexible Two-Dimensional Ti n+ 1 C n (n= 1, 2 and 3) and Their Functionalized MXenes Predicted by Density Functional Theories. *Phys. Chem. Chem. Phys.* **2015**, *17*, 15348−15354.

(11) Jhon, Y.; Seo, M.; Jhon, Y. First-Principles Study of a MXene Terahertz Detector. *Nanoscale* **2018**, *10*, 69−75.

(12) Li, N.; Meng, Q.; Zhu, X.; Li, Z.; Ma, J.; Huang, C.; Song, J.; Fan, J. Lattice Constant-Dependent Anchoring Effect of MXenes for Lithium−Sulfur (Li−S) Batteries: A DFT Study. *Nanoscale* **2019**, *11*, 8485−8493.

(13) Guha, S.; Kabiraj, A.; Mahapatra, S. High-Throughput Design of Functional-Engineered MXene Transistors with Low-Resistive Contacts. *npj Comput. Mater.* **2022**, *8*, 202.

(14) Rems, E.; Anayee, M.; Fajardo, E.; Lord, R. L.; Bugallo, D.; Gogotsi, Y.; Hu, Y. J. Computationally Guided Synthesis of MXenes by Dry Selective Extraction. *Adv. Mater.* **2023**, *35*, 2305200.

(15) Tian, S.; Zhou, K.; Huang, C.-Q.; Qian, C.; Gao, Z.; Liu, Y. Investigation and Understanding of the Mechanical Properties of MXene by High-Throughput Computations and Interpretable Machine Learning. *Extreme Mech. Lett.* **2022**, *57*, 101921.
(16) Muraleedharan, M. G.; Kent, P. R. Novel Boron Nitride MXenes As Promising Energy Storage Materials. *Nanoscale* **2022**, *14*, 9086−9096.
(17) Khazaei, M.; Arai, M.; Sasaki, T.; Estili, M.; Sakka, Y. Two-Dimensional Molybdenum Carbides: Potential Thermoelectric Materials of the MXene Family. *Phys. Chem. Chem. Phys.* **2014**, *16*, 7841−7849.
(18) Zeng, Z.; Chen, X.; Weng, K.; Wu, Y.; Zhang, P.; Jiang, J.; Li, N. Computational Screening Study of Double Transition Metal Carbonitrides M′2M″CNO2-MXene As Catalysts for Hydrogen Evolution Reaction. *npj Comput. Mater.* **2021**, *7*, 80.
(19) Pandey, M.; Thygesen, K. S. Two-Dimensional MXenes As Catalysts for Electrochemical Hydrogen Evolution: A Computational Screening Study. *J. Phys. Chem. C* **2017**, *121*, 13593−13598.
(20) Yang, X.-Y.; Luo, W.; Ahuja, R. Fluoride Ion Batteries: Designing Flexible M2CH2 (M= Ti or V) MXenes As High-Capacity Cathode Materials. *Nano Energy* **2020**, *74*, 104911.
(21) Jin, D.; Johnson, L. R.; Raman, A. S.; Ming, X.; Gao, Y.; Du, F.; Wei, Y.; Chen, G.; Vojvodic, A.; Gogotsi, Y.; et al. Computational Screening of 2D Ordered Double Transition-Metal Carbides (MXenes) As Electrocatalysts for Hydrogen Evolution Reaction. *J. Phys. Chem. C* **2020**, *124*, 10584−10592.
(22) Adam, M. L.; Moses, O. A.; Mailoa, J. P.; Hsieh, C.-Y.; Yu, X.-F.; Li, H.; Zhao, H. Navigating Materials Chemical Space to Discover New Battery Electrodes Using Machine Learning. *Energy Storage Mater.* **2024**, *65*, 103090.
(23) Moses, I. A.; Joshi, R. P.; Ozdemir, B.; Kumar, N.; Eickholt, J.; Barone, V. Machine Learning Screening of Metal-Ion Battery Electrode Materials. *ACS Appl. Mater. Interfaces* **2021**, *13*, 53355−53362.
(24) Priya, P.; Nguyen, T. C.; Saxena, A.; Aluru, N. R. Machine Learning Assisted Screening of Two-Dimensional Materials for Water Desalination. *ACS Nano* **2022**, *16*, 1929−1939.
(25) Deng, B.; Zhong, P.; Jun, K.; Riebesell, J.; Han, K.; Bartel, C. J.; Ceder, G. CHGNet As a Pretrained Universal Neural Network Potential for Charge-Informed Atomistic Modelling. *Nat. Mach. Intell.* **2023**, *5*, 1031−1041.
(26) Xie, T.; Grossman, J. C. Crystal Graph Convolutional Neural Networks for an Accurate and Interpretable Prediction of Material Properties. *Phys. Rev. Lett.* **2018**, *120*, 145301.
(27) Sitapure, N.; Kwon, J. S.-I. CrystalGPT: Enhancing System-to-System Transferability in Crystallization Prediction and Control Using Time-Series-Transformers. *Comput. Chem. Eng.* **2023**, *177*, 108339.
(28) Sitapure, N.; Kwon, J. S.-I. Exploring the Potential of Time-Series Transformers for Process Modeling and Control in Chemical Systems: An Inevitable Paradigm Shift? *Chem. Eng. Res. Des.* **2023**, *194*, 461−477.
(29) Park, J.; Kim, M.; Kim, H.; Lee, J.; Lee, I.; Park, H.; Lee, A.; Min, K.; Lee, S. Exploring the Large Chemical Space in Search of Thermodynamically Stable and Mechanically Robust MXenes *via* Machine Learning. *Phys. Chem. Chem. Phys.* **2024**, *26*, 10769−10783.
(30) Vertina, E. W.; Deskins, N. A.; Sutherland, E.; Mangoubi, O. Predicting MXene Properties *via* Machine Learning. In *2022 21st IEEE International Conference on Machine Learning and Applications (ICMLA)*; IEEE, 2022; pp 1573−1578.
(31) He, M.; Zhang, L. Machine Learning and Symbolic Regression Investigation on Stability of MXene Materials. *Comput. Mater. Sci.* **2021**, *196*, 110578.
(32) Min, K.; Cho, E. Accelerated Discovery of Potential Ferroelectric Perovskite *via* Active Learning. *J. Mater. Chem. C* **2020**, *8*, 7866−7872.
(33) Sheng, Y.; Wu, Y.; Yang, J.; Lu, W.; Villars, P.; Zhang, W. Active Learning for the Power Factor Prediction in Diamond-Like Thermoelectric Materials. *npj Comput. Mater.* **2020**, *6*, 171.
(34) Choi, E.; Jo, J.; Kim, W.; Min, K. Searching for Mechanically Superior Solid-State Electrolytes in Li-Ion Batteries *via* Data-Driven Approaches. *ACS Appl. Mater. Interfaces* **2021**, *13*, 42590−42597.
(35) Flores, R. A.; Paolucci, C.; Winther, K. T.; Jain, A.; Torres, J. A. G.; Aykol, M.; Montoya, J.; Nørskov, J. K.; Bajdich, M.; Bligaard, T. Active Learning Accelerated Discovery of Stable Iridium Oxide Polymorphs for the Oxygen Evolution Reaction. *Chem. Mater.* **2020**, *32*, 5854−5863.
(36) Rajan, A. C.; Mishra, A.; Satsangi, S.; Vaish, R.; Mizuseki, H.; Lee, K.-R.; Singh, A. K. Machine-Learning-Assisted Accurate Band Gap Predictions of Functionalized MXene. *Chem. Mater.* **2018**, *30*, 4031−4038.
(37) Ward, L.; Dunn, A.; Faghaninia, A.; Zimmermann, N. E.; Bajaj, S.; Wang, Q.; Montoya, J.; Chen, J.; Bystrom, K.; Dylla, M.; et al. Matminer: An Open Source Toolkit for Materials Data Mining. *Comput. Mater. Sci.* **2018**, *152*, 60−69.
(38) Li, X.; Huang, Z.; Shuck, C. E.; Liang, G.; Gogotsi, Y.; Zhi, C. MXene Chemistry, Electrochemistry and Energy Storage Applications. *Nat. Rev. Chem* **2022**, *6*, 389−404.
(39) Wang, L.; Gao, S.; Li, W.; Zhu, A.; Li, H.; Zhao, C.; Zhang, H.; Wang, W.-H.; Wang, W. Machine Learning Assisted Screening of MXenes Pseudocapacitive Materials. *J. Power Sources* **2023**, *564*, 232834.
(40) Wyatt, B. C.; Rosenkranz, A.; Anasori, B. 2D MXenes: Tunable Mechanical and Tribological Properties. *Adv. Mater.* **2021**, *33*, 2007973.
(41) Gjerding, M. N.; Taghizadeh, A.; Rasmussen, A.; Ali, S.; Bertoldo, F.; Deilmann, T.; Knøsgaard, N. R.; Kruse, M.; Larsen, A. H.; Manti, S.; et al. Recent Progress of the Computational 2D Materials Database (C2DB). *2D Mater.* **2021**, *8*, 044002.
(42) Yan, T.; Xiao, M.; Song, H.; Lv, Y.; Li, Z.; Xiao, B. S-and Cl-Functionalized Nb 2 C MXenes As Novel Anode Materials for Sodium-Ion Batteries: A First-Principles Study. *New J. Chem.* **2023**, *47*, 6412−6419.
(43) Wang, L.; Chang, W.-L.; Sun, Z.-Q.; Zhang, Z.-M. Investigations on the Thermoelectric and Thermodynamic Properties of Y 2 CT 2 (T= O, F, OH). *RSC Adv.* **2022**, *12*, 14377−14383.
(44) Kamysbayev, V.; Filatov, A. S.; Hu, H.; Rui, X.; Lagunas, F.; Wang, D.; Klie, R. F.; Talapin, D. V. Covalent Surface Modifications and Superconductivity of Two-Dimensional Metal Carbide MXenes. *Science* **2020**, *369*, 979−983.
(45) Li, M.; Li, X.; Qin, G.; Luo, K.; Lu, J.; Li, Y.; Liang, G.; Huang, Z.; Zhou, J.; Hultman, L.; et al. Halogenated Ti3C2MXenes with Electrochemically Active Terminals for High-Performance Zinc Ion Batteries. *ACS Nano* **2021**, *15*, 1077−1085.
(46) Li, Y.; Shao, H.; Lin, Z.; Lu, J.; Liu, L.; Duployer, B.; Persson, P. O.; Eklund, P.; Hultman, L.; Li, M.; et al. A General Lewis Acidic Etching Route for Preparing MXenes with Enhanced Electrochemical Performance in Non-Aqueous Electrolyte. *Nat. Mater.* **2020**, *19*, 894−899.
(47) Chang, W.-L.; Sun, Z.-Q.; Zhang, Z.-M.; Wei, X.-P.; Tao, X. Thermoelectric Properties of Two-Dimensional Double Transition Metal MXenes: ScYCT2 (T= F, OH). *J. Phys. Chem. Solids* **2023**, *176*, 111210.
(48) He, Q.; Hu, H.; Han, J.; Zhao, Z. Double Transition-Metal TiVCTX MXene with Dual-Functional Antibacterial Capability. *Mater. Lett.* **2022**, *308*, 131100.
(49) Anasori, B.; Xie, Y.; Beidaghi, M.; Lu, J.; Hosler, B. C.; Hultman, L.; Kent, P. R.; Gogotsi, Y.; Barsoum, M. W. Two-Dimensional, Ordered, Double Transition Metals Carbides (MXenes). *ACS Nano* **2015**, *9*, 9507−9516.
(50) Ma, Q.; Zhang, Z.; Kou, P.; Wang, D.; Wang, Z.; Sun, H.; Zheng, R.; Liu, Y. *In-Situ* Synthesis of Niobium-Doped TiO2 Nanosheet Arrays on Double Transition Metal MXene (TiNbCTx) As Stable Anode Material for Lithium-Ion Batteries. *J. Colloid Interface Sci.* **2022**, *617*, 147−155.
(51) Zhu, S.-Y.; Li, Y.-Q.; Wang, X.-Y.; Tang, D.-S.; He, Q.-W.; Liu, C.; Liu, F.-C.; Wang, X.-C. Theoretical Investigations of Sc2C Based

https://doi.org/10.1021/acsnano.4c08621
ACS Nano XXXX, XXX, XXX−XXX

Functionalized MXenes for Applications in Nanoelectromechanical Systems. *Phys. E* **2023**, *145*, 115491.
(52) Modi, N.; Naik, Y.; Khengar, S.; Jariwala, P.; Shah, D.; Thakor, P. Theoretical Investigations of Asymmetric Functionalized Y2C-Based MXene Monolayers. *Solid State Commun.* **2023**, *372*, 115303.
(53) Muhammed, M.; Mokkath, J. Surface Termination Dependent Optical Characteristics of MXene Nanoflakes. *Mater. Today Chem.* **2023**, *29*, 101447.
(54) Xin, C.; Fan, Z.; Sun, Z.; Li, H.; Jin, G.; Pan, F.; Sui, Y. Asymmetric Janus Functionalization Induced Magnetization and Switchable Out-of-Plane Polarization in 2D MXene Mo 2 CXX. *Phys. Chem. Chem. Phys.* **2023**, *25*, 8676−8683.
(55) Siriwardane, E. M. D.; Hu, J. First-Principles Investigation of Ti2CSO and Ti2CSSe Janus MXene Structures for Li and Mg Electrodes. *J. Phys. Chem. C* **2021**, *125*, 12469−12477.
(56) Jang, C. W.; Lee, W. J.; Kim, J. K.; Park, S. M.; Kim, S.; Choi, S.-H. Growth of Two-Dimensional Janus MoSSe by a Single *In Situ* Process without Initial or Follow-Up Treatments. *NPG Asia Mater.* **2022**, *14*, 15.
(57) Harris, S. B.; Lin, Y.-C.; Puretzky, A. A.; Liang, L.; Dyck, O.; Berlijn, T.; Eres, G.; Rouleau, C. M.; Xiao, K.; Geohegan, D. B. Real-Time Diagnostics of 2D Crystal Transformations by Pulsed Laser Deposition: Controlled Synthesis of Janus WSSe Monolayers and Alloys. *ACS Nano* **2023**, *17*, 2472−2486.
(58) Zhang, L.; Yu, J.; Yang, M.; Xie, Q.; Peng, H.; Liu, Z. Janus Graphene from Asymmetric Two-Dimensional Chemistry. *Nat. Commun.* **2013**, *4*, 1443.
(59) Holm, A.; Park, J.; Goodman, E. D.; Zhang, J.; Sinclair, R.; Cargnello, M.; Frank, C. W. Synthesis, Characterization, and Light-Induced Spatial Charge Separation in Janus Graphene Oxide. *Chem. Mater.* **2018**, *30*, 2084−2092.
(60) Lee, J. A.; Park, J.; Choi, Y. T.; Kim, R. E.; Jung, J.; Lee, S.; Seo, M. H.; Kim, H. S. Influence of Tensile Properties on Hole Expansion Ratio Investigated Using a Generative Adversarial Imputation Network with Explainable Artificial Intelligence. *J. Mater. Sci.* **2023**, *58*, 4780−4794.
(61) Kim, H.; Na, J.; Lee, W. B. Generative Chemical Transformer: Neural Machine Learning of Molecular Geometric Structures from Chemical Language *via* Attention. *J. Chem. Inf. Model.* **2021**, *61*, 5804−5814.
(62) Lee, C. H.; Pahari, S.; Sitapure, N.; Barteau, M. A.; Kwon, J. S.-I. Investigating High-Performance Non-Precious Transition Metal Oxide Catalysts for Nitrogen Reduction Reaction: A Multifaceted DFT−kMC−LSTM Approach. *ACS Catal.* **2023**, *13*, 8336−8346.
(63) Chutia, A.; Thetford, A.; Stamatakis, M.; Catlow, C. R. A. A DFT and KMC Based Study on the Mechanism of the Water Gas Shift Reaction on the Pd (100) Surface. *Phys. Chem. Chem. Phys.* **2020**, *22*, 3620−3632.
(64) Lee, C. H.; Pahari, S.; Sitapure, N.; Barteau, M. A.; Kwon, J. S.-I. DFT−kMC Analysis for Identifying Novel Bimetallic Electrocatalysts for Enhanced NRR Performance by Suppressing HER at Ambient Conditions *via* Active-Site Separation. *ACS Catal.* **2022**, *12*, 15609−15617.
(65) Jain, A.; Ong, S. P.; Hautier, G.; Chen, W.; Richards, W. D.; Dacek, S.; Cholia, S.; Gunter, D.; Skinner, D.; Ceder, G.; Persson, K. A. Commentary: The Materials Project: A Materials Genome Approach to Accelerating Materials Innovation. *APL Mater.* **2013**, *1*, 011002.
(66) Ong, S. P.; Richards, W. D.; Jain, A.; Hautier, G.; Kocher, M.; Cholia, S.; Gunter, D.; Chevrier, V. L.; Persson, K. A.; Ceder, G. Python Materials Genomics (pymatgen): A Robust, Open-Source Python Library for Materials Analysis. *Comput. Mater. Sci.* **2013**, *68*, 314−319.
(67) Hohenberg, P.; Kohn, W. Inhomogeneous Electron Gas. *Phys. Rev.* **1964**, *136*, B864−B871.
(68) Kresse, G.; Furthmuller, J. Efficient Iterative Schemes for *Ab Initio* Total-Energy Calculations Using a Plane-Wave Basis Set. *Phys. Rev. B: Condens. Matter Mater. Phys.* **1996**, *54*, 11169−11186.
(69) Blöchl, P. E. Projector Augmented-Wave Method. *Phys. Rev. B: Condens. Matter Mater. Phys.* **1994**, *50*, 17953−17979.
(70) Kresse, G.; Joubert, D. From Ultrasoft Pseudopotentials to the Projector Augmented-Wave Method. *Phys. Rev. B: Condens. Matter Mater. Phys.* **1999**, *59*, 1758−1775.
(71) Perdew, J. P.; Burke, K.; Ernzerhof, M. Generalized Gradient Approximation Made Simple. *Phys. Rev. Lett.* **1996**, *77*, 3865−3868.
(72) Dudarev, S. L.; Botton, G. A.; Savrasov, S. Y.; Humphreys, C. J.; Sutton, A. P. Electron-Energy-Loss Spectra and the Structural Stability of Nickel Oxide: An LSDA+U Study. *Phys. Rev. B: Condens. Matter Mater. Phys.* **1998**, *57*, 1505−1509.

https://doi.org/10.1021/acsnano.4c08621
ACS Nano XXXX, XXX, XXX−XXX